Decorrelating Remote Sensing Color Bands From Bathymetry in Optically Shallow Waters

Christopher L. Conger, Eric J. Hochberg, Charles H. Fletcher, III, and Marlin J. Atkinson

***Abstract*—We have developed a simple technique to decorrelate remote sensing color band data from depth in optically shallow water. The method linearizes color band data with respect to depth by subtracting an optically deepwater value from the entire waveband under consideration and taking the natural logarithm of the result. Next, this linearized waveband is rotated about the model 2 regression line computed against a bathymetry band. The rotated color band is decorrelated from water depth. We demonstrate the technique for a small area of Kailua Bay, Oahu, HI, using Quickbird multispectral and Scanning Hydrographic Operational Airborne Lidar Survey LIDAR data. Results indicate that color band data are effectively decorrelated from depth, while bottom reflector variability is maintained, thus providing the basis for further analysis of the depth-invariant wavebands. The primary benefit of our technique is that wavebands are rotated independently, preserving relative spectral information.**

***Index Terms*—Bathymetry, coastal remote sensing, Kailua Bay, LIDAR, Quickbird, radiative transfer, reflectance.**

I. Introduction

REMOTE sensing has long been a useful tool for study of coastal benthic environments (reviewed in [1]). Numerous case studies point to the ability of remote sensing technology to provide meaningful, quantitative data on ecological and geomorphological systems [2]–[8]. Research into the technology itself has generated practical techniques for processing aquatic remote sensing imagery [9]–[13] and for linking optical remote sensing data with biophysical sea floor parameters [14]–[18]. The primary hindrance to routine use of remote sensing for study of optically shallow benthic environments is the presence of a highly (relative to air) absorbing and scattering water column of variable depth [19]. The remote sensing problem is to deconvolve these unknown radiative transfer effects from an unknown and variable sea-floor albedo signal.

Manuscript received January 4, 2005; revised November 23, 2005. This work was supported by the University of Hawaii School of Ocean and Earth Science and Technology contribution 6718 and Hawaii Institute of Marine Biology contribution 1219. The work of C. L. Conger was supported by the Office of Naval Research (ONR) under Award N00014-02-1-0799. The work of E. J. Hochberg was supported in part by the ONR under Award N00014-04-1-0361 and in part by the National Aeronautics and Space Administration under Grant NAG1-23445. The work of C. H. Fletcher was supported by the U.S. Geological Survey under Award 03WRAG0039. The work of M. J. Atkinson was supported by the ONR under Award N00014-04-1-0361.

C. L. Conger and C. H. Fletcher, III are with the Department of Geology and Geophysics, School of Ocean and Earth Science and Technology, University of Hawaii, Honolulu, HI 96822 USA (e-mail: conger@hawaii.edu; fletcher@soest.hawaii.edu).

E. J. Hochberg and M. J. Atkinson are with the Hawaii Institute of Marine Biology, School of Ocean and Earth Science and Technology, University of Hawaii, Kaneohe, HI 96744 USA (e-mail: hochberg@hawaii.edu; mja@hawaii.edu).

Digital Object Identifier 10.1109/TGRS.2006.870405

The most commonly cited approach to compensate for water column radiative transfer effects is that of Lyzenga [12], [20], [21]. This simple physics-based technique is derived from two-flow irradiance transfer and exploits the intrinsic correlation between two color bands to generate a psuedo-depth and a pseudocolor band. First, for each image color band, the signal from an optically deep portion of the scene is subtracted from the entire band, and the difference is ln-transformed. This transformation has the effect of (approximately) linearizing the data with respect to depth. Next, a model 2 regression is performed on two of the ln-transformed color bands, and the bands are rotated so that the regression slope becomes the abscissa in a new coordinate system. This new abscissa is primarily related to variations in water depth, while the orthogonal ordinate axis is primarily related to variations in bottom albedo for the convolved color bands. Theoretically, the psuedo-depth channel can be calibrated with appropriate ground truth information to provide absolute depth, and the pseudocolor channel is a depth-invariant index of sea-floor composition.

While it has proven to be a useful processing step [7], there are complications associated with Lyzenga's method. First, the computed pseudodepth channel is dependent on the relationship between bottom albedos in the two color bands. The result is that different bottom-types at the same actual depth appear at different pseudodepths. More importantly, since it is a rotation of a convolution of two wavebands, it is difficult to interpret a physical basis for the psuedo-color band. Advancements on Lyzenga's basic model include the recognition that water column optical properties can be spatially heterogeneous within a scene [22]. Other researchers have focused on merging external bathymetry data with Lyzenga rotation results, thus providing absolute calibration for the pseudodepth channel and creating a bathymetric chart at the resolution of the digital image data [23]–[26].

We present a new method for decorrelating remote sensing color bands from bathymetry, inspired both by Lyzenga's rotation approach and by efforts to merge LIDAR bathymetry data with color band data. Modern LIDAR systems have the ability to generate data at meter-scale spatial resolution, which is near that of high-resolution satellite image systems such as Ikonos (4 m) and Quickbird (2.4 m). Availability of such high-resolution data removes the need for computing water depth from passive imaging data, yet there is still a need to compensate for water column radiative transfer effects in the color-band data. Our approach is to linearize color bands with respect to depth following Lyzenga's method. However, rather than rotating two color bands about the regression slope, we rotate a single color band against the high-resolution bathymetry. In the resulting co-

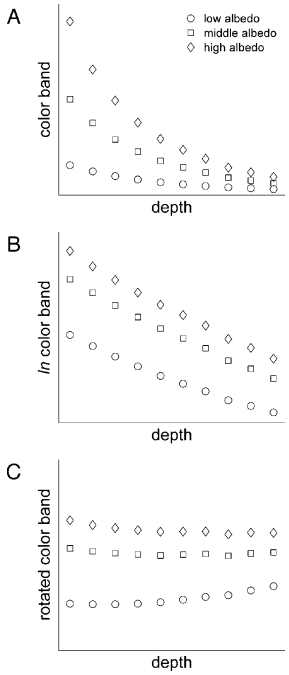

Fig. 1. Conceptual model for decorrelating color band data from depth. (a) Within a given waveband, the bottom-reflected radiance signal decreases approximately exponentially with depth. Deviations from exponential decay are due to scattering effects. Values shown here are modeled using Hydrolight 4.1 forward radiative transfer model. (b) After subtracting the value for optically deep water, the natural logarithm of the bottom-reflected signal decreases approximately linearly with water depth. Different bottom albedos appear as parallel lines with the same slope. (c) Rotating the axes through the angle defined by the slope effectively decorrelates color band data from depth, while maintaining the relative intensities of different bottom albedos.

ordinate system, the ordinate axis represents color band data decorrelated from water depth: for a given bottom reflector-type (i.e., a constant albedo), intensity in the rotated color band is independent of water depth. We demonstrate this technique using Quickbird satellite imagery and a Scanning Hydrographic Operational Airborne Lidar Survey (SHOALS) LIDAR interpolated bathymetry surface.

II. Materials and Methods

A. Model

For a given color band, the remotely sensed signal (less atmospheric and sea surface effects) can be modeled as a linear function of bottom albedo and an exponential function of water depth [Fig. 1(a)] [19]. Variations from the exponential decay are due to backscattering in the water column. Taking the natural logarithm of the remotely sensed signal has the effect of (approximately) linearizing the color band data with respect to depth [Fig. 1(b)]. Computing the model 2 linear regression between the ln-transformed color band and depth, and rotating the coordinate system about that regression line decorrelates the color band data from water depth [Fig. 1(c)]. In other words, by rotating the ln-transformed color band according to its linear relationship with depth, we are left with a color band whose intensity no longer decreases with increasing depth. The decorrelated color band data do not have physically meaningful units, but can be calibrated to absolute albedo using techniques such as the empirical line method. This model requires that bathymetry information exists for each pixel in the color bands.

An important component of our model is the data from which we compute the model 2 linear regression. Considering an entire coastal scene, several different bottom-types are present, represented by different bottom albedos. After linearization, these albedos form roughly parallel lines, as in Fig. 1(b). If all bottom albedos are equally present at all depths under consideration, then a regression computed for all pixels will return the correct slope. However, if some albedos are not present, then the regression line becomes skewed toward those albedos that are present. For example, if the first several "low albedo" points in Fig. 1(b) were missing, then the regression slope would be more strongly negative. That is, variability in the data is due to both bottom composition and water optical depth. Since our goal is to remove the variability due to depth while maintaining variability due to bottom composition, it is advantageous to compute the regression line using only a single bottom reflector-type [7] that is present throughout the scene. Then, the entire scene may be rotated about the regression line.

B. Data

We demonstrated this technique using two independent data sets for Kailua Bay, Oahu, Hawaii [Fig. 2(a)]: 1) a Quickbird image acquired March 13, 2003 (scene ID 03MAR13 205 953) and 2) SHOALS LIDAR bathymetry data acquired in 1999. Three bands were used from the Quickbird image: blue (450–520 nm), green (520–600 nm), and red (630–690 nm). The Quickbird scene exhibited excellent environmental quality, with very high water clarity, few breaking waves, no visible surface gravity waves, negligible glint, and almost no cloud cover. The image was georectified with a resolution of 2.4 m per pixel. For this study, we considered only the three visible wavebands in a 1500×1000 pixel subset of the image at the northern end of the Kailua Bay, extending from shore to optically deep water [Fig. 2(b)]. The average distance between the irregularly spaced, nongridded SHOALS data points was 2.8 m. We used a continuous curvature surface gridding algorithm (Generic Mapping Tools' surface function) to rasterize the LIDAR data, creating a bathymetric surface at the same 2.4-m pixel resolution as, and coregistered with, the Quickbird data [Fig. 2(c)]. We created an image mask to remove the influence of clouds, subaerial surfaces, and artifacts in the bathymetric surface from the analyzed portion of the image, leaving 1 055 157 pixels for evaluation.

C. Processing

Following Lyzenga [12], [20], [21] for each color band, we determined the minimum value from a portion of the scene covering optically deep water. We subtracted this deep-water value from the entire color band then computed the natural logarithm. To constrain the model 2 regression, we defined a region of interest in a nearshore-to-offshore transect that encompassed 2164 pixels of carbonate sand (a relatively homogeneous reflector), with depths ranging from near sea level to 20 m [Fig. 2(b)]. Using these transect pixels, we performed a regression for each color band against corresponding depth values extracted from the SHOALS image. Since these are two-variable systems, we

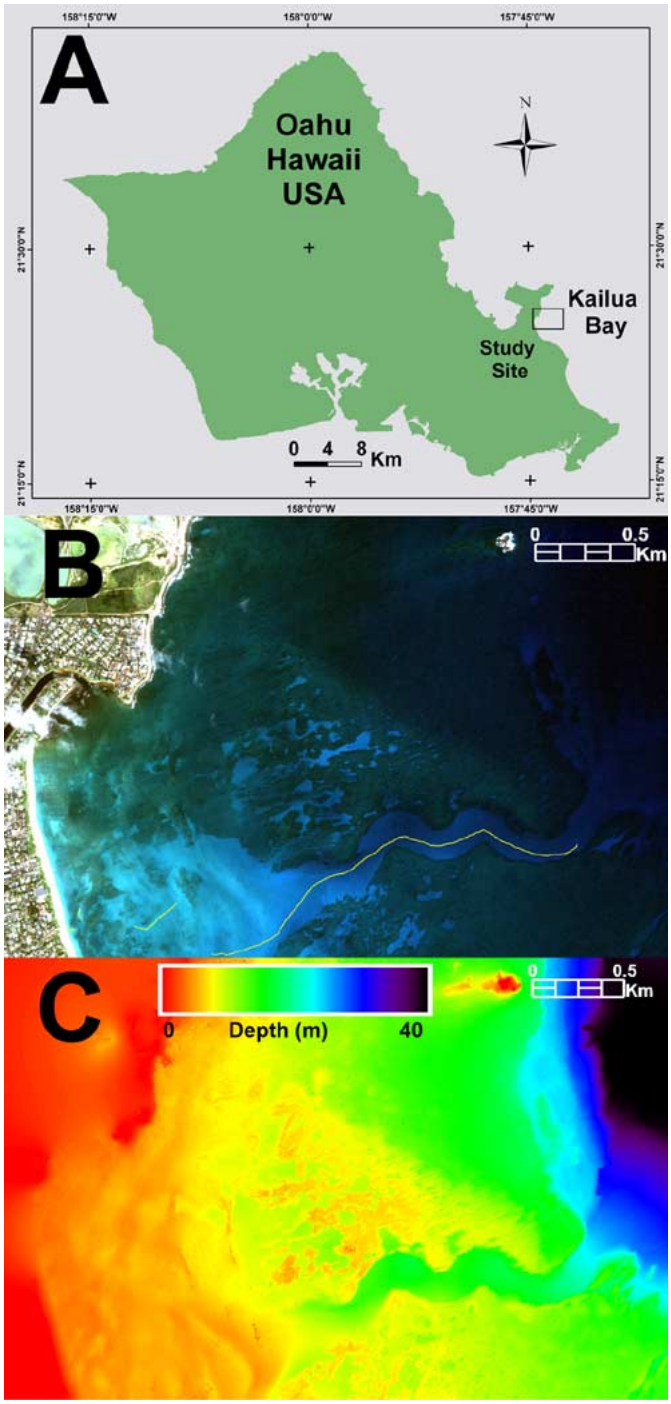

Fig. 2. Study site location and data. (a) Map of Oahu, Hawaii. Study site within Kailua Bay is outlined. (b) Initial QuickBird image for study site, displayed as an RGB image. Sand transect data was collected from pixels under the yellow lines. (c) Shoals LIDAR data interpolated to a depth image and displayed in rainbow hues varying from red at 0 m to purple at 20 m.

used principal component analysis to compute the perpendicular regression coefficients [27]. The first principal component described the major axis of the bivariate data, which in this case represented the attenuation of signal with depth. The orthogonal second component described the minor axis of the bivariate data, in this case variations of signal within the homogeneous sand reflector-type. This second principal component provided the rotation coefficients to rotate the entire ln-transformed color band, thus decorrelating it from depth. To quantify the utility of rotation, we computed the correlation of each color band with depth before and after rotation, using the transect pixels.

III. Results

Fig. 3 shows the sand transect pixels for each color band plotted against depth at each processing step: initial data [Fig. 3(a)], ln-transformed data [Fig. 3(b)], and rotated data [Fig. 3(c)]. These graphs illustrate decorrelation in both blue and green bands, and a lack of decorrelation in the red band. Fig. 4 shows gray-scale images of each color band before and after processing. Rotation greatly enhances contrast of bottom features in the blue and green bands, while the rotated red band exhibits mostly noise. For sand transect pixels, correlation coefficients with depth before rotation (and after ln-transformation) are 0.979, 0.991, and 0.857 for the blue, green, and red bands, respectively. After rotation, correlation coefficients are 0.001, 0.002, and 0.012 for the blue, green, and red bands, respectively. Rotation clearly decorrelates the blue and green bands from water depth. While the after-rotation correlation value for the red band is much smaller than the before-rotation correlation value, examination of Figs. 3(c) and 4(f) reveals that rotation coefficients computed from pixels in optically deep waters is not a viable product.

IV. Discussion

Our proposed technique relies on the strong linear relationship between ln-transformed color bands and depth in optically shallow water. We have invoked a simplified two-flow irradiance transfer model as the physical basis for this relationship. Maritorena *et al.* [19] provide an excellent derivation of the model and clearly demonstrate its utility for describing shallow water reflectance. To the best of our knowledge, all case studies on the matter have found the model's approximations to be perfectly adequate (e.g., [7], [9], and [12]), despite the fact that most remote sensing studies consider radiance (often in units of digital counts) as opposed to irradiance or reflectance. It is nevertheless important to understand that this is a one-dimensional model, describing only the vertical variation of light within the water column, including the seafloor.

The first implication is that the atmosphere and sea surface are not included. Prior to application of the model, compensation must be provided for nonwater column radiative transfer effects such as aerosol scattering or sun glint. Algorithms exist for such compensations (e.g., [11] and [28]). For the image used in this study, only minor glint effects are present, and subtracting deep-water radiance from the entire scene acts as a zero-order atmospheric correction.

The second implication is that the model assumes a vertically homogeneous water column with respect to optical properties. The coastal zone is often a complex hydrodynamic environment, resulting in vertical variations of biotic and abiotic optically significant water column constituents. However, Maritorena *et al.* [19] point out that it is possible to assume a "bulk" attenuation that describes the entire water column. In fact, our method does not rely on knowledge of actual attenuation values, but simply that attenuation is approximately exponential through the water column considered as a whole. Deviation from this exponential

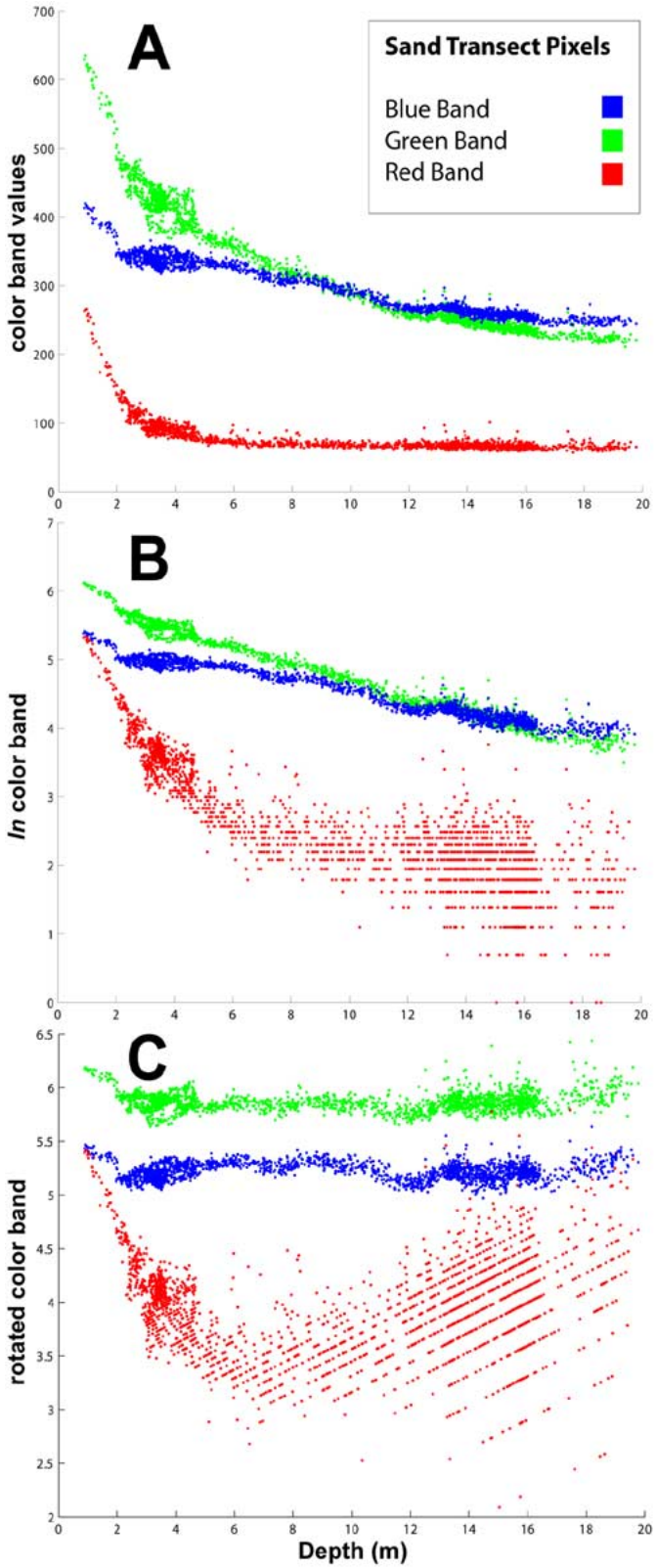

Fig. 3. Plots of sand transect pixels for each stage of the process. (a) Initial data. Sand transect pixels for blue, green, and red bands are plotted with depth values on the x axis and DN values on the y axis. (b) Log-transformed data. Sand transect pixels are plotted with depth values on the x axis and ln-transformed DN values on the y axis. (c) Rotated data. Sand transect pixels are plotted with depth values on the x axis and rotated color band values on the y axis.

attenuation, as may occur in vertically stratified waters, has the potential to detrimentally affect the technique.

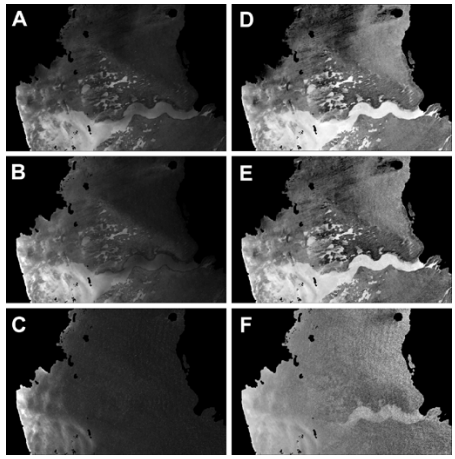

Fig. 4. Gray-scale images of initial color bands and rotated color bands. All images are masked to remove all terrestrial components, anomalies in the depth data, and surface disturbances on the water. (a) Initial blue band. (b) Initial green band. (c) Initial red band. (d) Rotated blue band. (e) Rotated green band. (f) Rotated red band.

The final implication of the model is that it does not account for horizontal variation in water column optical properties. That is, we assume that attenuation is constant throughout the scene. For the present study, this is a reasonable assumption, given the excellent environmental conditions under which the imagery was acquired: the study area is small, Kailua Bay is open to the ocean, allowing significant water exchange, and neither wind nor surface gravity waves are present in the image, with no apparent sediment resuspension. However, just as optical properties vary vertically around coral reefs, they also vary horizontally across spatial scales of tens of meters to kilometers [29], [30]. Such variability must be considered before application of this model. If significant variability is found, then the image may be divided into subsets, each with relatively constant optical properties, or algorithms may be applied which automatically account for such variability, such as that proposed by Tassan [22].

Another important consideration for application of this method is the depth-of-detection limit, which is the depth where the seafloor-returned signal is no longer strong enough to provide for bottom detection and/or discrimination. In this study, the linear relationship between ln-transformed color bands and depth is clearly apparent in both the blue and green, but is notably absent in the red [Fig. 3(b)]. Examination of the data reveals that the blue and green bands exhibit strong seafloor-return signals ($\mathrm{SNR} \sim 100$) to depths of 40 and 25 m, respectively, while the red band loses the seafloor signal at only 5-m depth [Figs. 3 and 4(c)]. For most of the scene under consideration, the balance of variability in the red channel is comprised of sea surface clutter and sensor noise. Thus, it is inappropriate to apply the rotation to this channel, and the appearance of seafloor features in the rotated red band [Fig. 4(f)] is an artifact of the lack of decorrelation from the depth band.

Discounting environmental and sensor noise, variability in the color bands comes from two sources. First, and most significant, is attenuation due to water optical depth. For an homogenous bottom-type, and therefore a relatively homogenous reflector, Fig. 3(a) indicates ranges of approximately 150, 400,

and 200 digital counts for the blue, green, and red color bands, respectively, across the depths considered in this study. The second source of variability arises from differences in reflector type. The green band in Fig. 3(a) shows a range of about 75 digital counts near 4-m depth, indicating local differences in sand albedo in those pixels. After rotation, Fig. 3(c) still shows this local variation, but the global depth-dependent variation is no longer present. Thus, this technique effectively removes variations due to water depth, while maintaining variations due to bottom signal.

Removal of variation associated with water depth is possible because of the approximately linear relationship between ln-transformed reflectance and water depth, as measured by the correlation coefficient. High correlation coefficients, 0.979 and 0.991 measured for the sand pixels in blue and green ln-transformed bands respectively, indicate an almost perfect linear relationship [Fig. 3(b)]. In striking contrast are the same sand pixels in the ln-transformed red band. These pixels pass into optically deep waters by 5 m, no longer varying with depth and blowing up during the ln-transform. Though by other standards these pixels' correlation coefficient of 0.857 may seem high, in this case it is unacceptable by comparison to the almost perfect linear relationship exhibited when the bottom is in optically shallow waters. Consequently, after rotation the red sand pixels in Fig. 3(c) do not display the same narrow range of variation, resulting from minor differences in sand albedo, as do both blue and green. Fig. 3(c) is the product of pixel data in optically deep waters where the rotation coefficients are computed for sensor noise and surface clutter. Again, though a correlation coefficient of 0.012 may seem low by normal standards, in this case it is completely unacceptable.

The only discontinuity in the linear relationships of the blue and green ln-transformed sand pixels with depth is around 2 m. There is a slight steepening of the trend in this shallow region of the scene. One possible source for this discontinuity might be localized sediment resuspension from the higher energy environment of the near-shore breaker region. This would create different water column optical properties than the rest of the transect. Another possibility is that there may be a different type of sand, and subsequent albedo, in this region. Either or both of these could result in the minor change in slope in the shallowest 2 m of the scene.

The output of our technique is analogous to that of Lyzenga, in that both methods generate pseudocolor bands whose numerical values have no readily interpretable physical meaning. A distinction is that output from Lyzenga's method represents a convolution of two color bands, while output from ours is a set of independently decorrelated color bands. The principal advantage is that our method maintains the relative intensities of different bottom reflectors within the primary wavebands, which provides for more direct knowledge-based interpretation. There is also potential that our pseudocolor bands may be calibrated to absolute reflectance through techniques such as the empirical line method, thus allowing application of spectral classifiers built using libraries of *in situ* reflectance data.

Because it is a rotation of axes into a new coordinate system, this method requires a depth value for each pixel to be rotated. In this study we have a best case scenario: the footprint of the LIDAR data is very close to the pixel size of the multispectral image, and we therefore have accurate values with which to perform the rotation. It may be possible to utilize depth data from a lower resolution source, interpolating to the resolution of the color bands. Provided that the interpolated surface adequately (though "adequate" has yet to be quantified) represents actual depth variations, rotation should provide significant decorrelation.

In summary, we have developed a method to decorrelate color band data from depth in optically shallow water. The method follows ideas introduced by Lyzenga [12], [20], [21], but differs in that individual ln-transformed color bands are rotated against a bathymetry band rather than other color bands. The method produces pseudocolor bands that are suitable for direct knowledge-based interpretation or for calibration to absolute reflectance. Since this model will work on any single color band that is paired with known depths, its utility is not limited by number or range of color bands, but rather by depth-of-detection within each band. The immediate effect of band rotation is that an object exhibits the same relative reflectance (i.e., pseudocolor) regardless of the depth at which it resides. As with Lyzenga's method, this simplifies the training data necessary for wholly empirical "sensor-down" image-based classifiers, which otherwise would require training of that object at different depths [31]. More importantly, this band rotation can serve as an intermediate step in deriving absolute seafloor reflectance imagery. Such imagery is basic input to "reef-up" classification in which independently acquired spectral libraries are used to train image classifiers [31]. Thus, image classification becomes a semi-analytical process that is not tied to a single scene.

ACKNOWLEDGMENT

LIDAR data provided courtesy of the U.S. Geological Survey, and DigitalGlobe provided Quickbird data. Fieldwork was supported by the U.S. Geological Survey. C. L. Conger thanks N. Frazer, Ph.D. (University of Hawaii) for both his insight and his questions.

REFERENCES

[1] E. P. Green, P. J. Mumby, A. J. Edwards, and C. D. Clark, "A review of remote sensing for the assessment and management of tropical coastal resources," *Coastal Manag.*, vol. 24, pp. 1–40, 1996.

[2] W. Ahmed and D. T. Neil, "An evaluation of LANDSAT Thematic Mapper (TM) digital data for discriminating coral reef zonation: Heron reef (GBR)," *Int. J. Remote Sens.*, vol. 15, no. 13, pp. 2583–2597, 1994.

[3] S. Andréfouët *et al.*, "Multi-site evaluation of IKONOS data for classification of tropical coral reef environments," *Remote Sens. Environ.*, vol. 88, no. 1, pp. 128–143, 2003.

[4] M. J. Atkinson and R. W. Grigg, "Model of a coral reef ecosystem. II. Gross and net benthic primary production at French Frigate Shoals, Hawaii," *Coral Reefs*, vol. 3, pp. 13–22, 1984.

[5] R. T. Bina, K. Carpenter, Z. Wolfgang, R. Jara, and J. B. Lim, "Coral reef mapping using LANDSAT data: Follow-up studies," in *Proc. 12th Int. Symp. Remote Sensing Environment*, vol. 3, 1978, pp. 2051–2070.

[6] W. Bour, L. Loubersac, and P. Raul, "Thematic mapping of reefs by processing of simulated SPOT satellite data: Application to the Trochus niloticus biotope on Tetembia Reef (New Caledonia)," *Marine Ecol. Prog. Ser.*, vol. 34, pp. 243–249, 1986.

[7] P. J. Mumby, E. P. Green, C. D. Clark, and A. J. Edwards, "Digital analysis of multispectral airborne imagery of coral reefs," *Coral Reefs*, vol. 17, no. 1, pp. 59–69, Mar. 1998.

[8] V. E. Smith, "Automated mapping and inventory of Great Barrier Reef zonation with LANDSAT data," *IEEE Ocean*, pp. 775–780, 1975.
[9] P. N. Bierwirth, T. J. Lee, and R. N. Burne, "Shallow sea-floor reflectance and water depth derived by unmixing multispectral imagery," *Photogramm. Eng. Remote Sens.*, vol. 59, no. 3, pp. 331–338, 1993.
[10] R. W. Gould and R. A. Arnone, "Remote sensing estimates of inherent optical properties in a coastal environment," *Remote Sens. Environ.*, vol. 61, pp. 290–301, 1997.
[11] E. J. Hochberg, S. Andréfouët, and M. R. Tyler, "Sea surface correction of high spatial resolution Ikonos images to improve bottom mapping in near-shore environments," *IEEE Trans. Geosci. Remote Sens.*, vol. 41, no. 7, pp. 1724–1729, Jul. 2003.
[12] D. Lyzenga, "Passive remote sensing techniques for mapping water depth and bottom features," *Appl. Opt.*, vol. 17, no. 3, pp. 379–383, 1978.
[13] C. M. Roelfsema, S. R. Phinn, and W. C. Dennison, "Spatial distribution of benthic microalgae on coral reefs determined by remote sensing," *Coral Reefs*, vol. 21, pp. 264–274, 2002.
[14] E. J. Hochberg and M. Atkinson, "Spectral discrimination of coral reef benthic communities," *Coral Reefs*, vol. 19, pp. 164–171, 2000.
[15] ——, "Capabilities of remote sensors to classify coral, algae, and sand as pure and mixed spectra," *Remote Sens. Environ.*, vol. 85, pp. 174–189, 2003.
[16] H. Holden and E. LeDrew, "Spectral discrimination of healthy and nonhealthy coral based on cluster analysis, principal component analysis, and derivative spectroscopy," *Remote Sens. Environ.*, vol. 65, pp. 217–224, 1998.
[17] M. R. Myers, H. T. Hardy, C. H. Mazel, and P. Dustan, "Optical spectra and pigmentation of Caribbean reef corals and macroalgae," *Coral Reefs*, vol. 18, pp. 179–186, 1999.
[18] S. J. Purkis and R. Pasterkamp, "Integrating *in situ* reef-top reflectance spectra with LANDSAT TM imagery to aid shallow-tropical benthic habitat mapping," *Coral Reefs*, vol. 23, no. 1, pp. 5–20, 2004.
[19] S. Maritorena, A. Morel, and B. Gentili, "Diffuse reflectance of oceanic shallow waters: Influence of water depth and bottom albedo," *Limnology Oceanog.*, vol. 39, no. 7, pp. 1689–1703, 1994.
[20] D. Lyzenga, "Shallow-water bathymetry using combined lidar and passive multispectral scanner data," *Int. J. Remote Sens.*, vol. 6, no. 1, pp. 115–125, 1985.
[21] ——, "Remote sensing of bottom reflectance and water attenuation parameters in shallow water using aircraft and LANDSAT data," *Int. J. Remote Sens.*, vol. 2, no. 1, pp. 71–82, 1981.
[22] S. Tassan, "Modified Lyzenga's method for macroalgae detection in water with nonuniform composition," *Remote Sens. Lett.*, pp. 1601–1607, 1996.
[23] L. L. Estep, W. J. Lillycrop, and L. E. Parson, "Sensor fusion for hydrographic applications," in *U. S. Army Corps of Engineers 1994 Training Symp.*, New Orleans, LA, 1994.
[24] M. Lee and G. Tuell, "A technique for generating bottom reflectance images from SHOALS data," in *U. S. Hydro 2003 Conf.*, Biloxi, 2003.
[25] J. Wozencraft, M. Lee, G. Tuell, and W. Philpot, "Use of shoals data to produce spectrally-derived depths in Kaneohe Bay, Hawaii," in *Proc. U.S. Hydro 2003 Conf.*, Biloxi, MS, 2003.
[26] L. Yarbrough and G. Easson, "Comparison of techniques for deriving bathymetry from remotely sensed data," in *AMRS Conf.: Hyperspectral Issues for Coastal Zone Environments*, 2003.
[27] A. Rencher, *Methods of Multivariate Analysis*, 2nd ed. New York: Wiley, 2002, ch. 12.
[28] S. Andréfouët, F. E. Muller-Karger, E. J. Hochberg, C. Hu, and K. L. Carder, "Change detection on shallow coral reef environments using LANDSAT ETM+ data," *Remote Sens. Environ.*, vol. 79, pp. 150–162, 2001.
[29] E. Karpouzli, "Underwater light characterization for correction of remotely sensed images," *Int. J. Remote Sens.*, vol. 24, pp. 2683–2702, 2003.
[30] S. Maritorena and N. Guillocheau, "Optical properties of water and spectral light absorption by living and nonliving particles and by yellow substances in coral reef waters of French Polynesia," *Marine Ecol. Prog. Ser.*, vol. 131, pp. 245–255, 1996.
[31] S. Purkis, "A 'reef-up' approach to classifying coral habitats from Ikonos imagery," *IEEE Trans. Geosci. Remote Sens.*, vol. 43, no. 6, pp. 1375–1390, Jun. 2005.

Christopher L. Conger, photograph and biography not available at the time of publication.

Eric J. Hochberg, photograph and biography not available at the time of publication.

Charles H. Fletcher, III, photograph and biography not available at the time of publication.

Marlin J. Atkinson, photograph and biography not available at the time of publication.